



Introducing a novel nanocomposite consisting of TiO₂ nanoparticles@ copper oxide/reduced graphene oxide for the electrocatalytic sensing of ascorbic acid

Mohammad Hossein Ghanbari¹ · Mohammad Hossein Mashhadizadeh¹ · Zahra Norouzi²

Received: 16 July 2020 / Accepted: 1 November 2020 / Published online: 20 November 2020
© Iranian Chemical Society 2020

Abstract

In the present work, titania nanoparticles (TiO₂NPs), copper oxide (CuO), and reduced graphene oxide (rGO) ternary nanocomposite (TiO₂NP@CuO-rGO)-modified glassy carbon electrode (GCE) have been used for sensitive detection and determination of ascorbic acid (AA). The modified glassy carbon electrode was characterized over the successive modification steps, by scanning electron microscope (SEM) imaging, FT-IR spectroscopy, XRD, cyclic voltammetry (CV), and electrochemical impedance spectroscopy (EIS). Electrochemical detection and determinations were made using differential pulse voltammetry (DPV), and the amount of ternary nanocomposite (TiO₂NP@CuO-rGO), the effect of pH, and potential scan rate were optimized. The electrochemical properties of the AA at the proposed modified electrode were monitored by performing CV experiments. The DPVs and CVs displayed one oxidation peak during the anodic potential scan. The electrochemical detection and determination by DPV provided a linear concentration range from 10.0 pM to 10.0 μM with a limit of detection (LOD) 3.0 pM. The TiO₂NP@CuO-rGO/GCE sensor demonstrated good reproducibility, stability, and repeatability and no interference in the electrochemical detection and determination of AA in the presence of many compounds. The suggested method was satisfactory practical for the detection and determination of AA in human synthetic blood serum samples, with recoveries about 99.2%.

Electronic supplementary material The online version of this article (<https://doi.org/10.1007/s13738-020-02114-7>) contains supplementary material, which is available to authorized users.

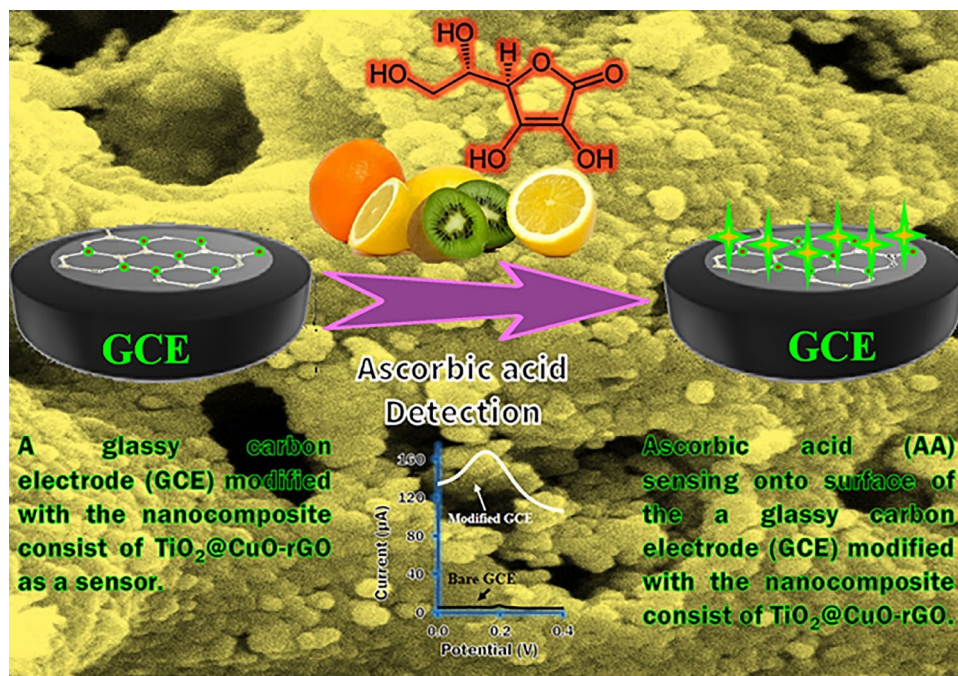
✉ Mohammad Hossein Ghanbari
ghanbari_khat@yahoo.com

¹ Faculty of Chemistry, Kharazmi University,
15719-14911 Tehran, Iran

² Faculty of Chemistry, University of Kashan,
87317-51167 Kashan, Iran

Graphic abstract

Titania nanoparticles@copper oxide–reduced graphene oxide: $\text{TiO}_2\text{NP}@\text{CuO-rGO}$. Applicability of the $\text{TiO}_2\text{NP}@\text{CuO-rGO}$ nanocomposite in fabrication of an efficient ascorbic acid (AA) sensor based on the use of a glassy carbon electrode.



Keywords Electrochemical sensor · Ascorbic acid · TiO_2 nanoparticles · Copper oxide · Reduced graphene oxide · $\text{TiO}_2\text{NP}@\text{CuO-rGO}$ nanocomposite

Introduction

The basic biologically active form of vitamin C is L-ascorbic acid (AA) (Scheme 1S). The biological activity of this vitamin is manifested as well as in its oxidation product, dehydroascorbic acid. While this vitamin is an essential water-soluble vitamin in human nutrition, humans do not have the necessary enzymes for its synthesis, albeit more animals can synthesize vitamin C from D-glucose. For the last step in this vitamin biosynthesis, enzyme l-gulono-gamma-lactone oxidase is essential but due to the inactivation of the Gulo gene by mutation more than 40 million years ago, humans must provide this nutrient from their diet exogenously [1].

Vitamin C or l-ascorbic acid takes part in numerous biochemical functions as a cofactor for different enzymes within the synthesis of adrenal and norepinephrine hormones, collagen, and metabolism of folic acid, tryptophan, and tyrosine [2, 3]. As a reducing agent in cellular metabolism, it is likewise significant for the absorption of iron in the gut and carnitine biosynthesis [4]. Fruits and vegetables, especially citrus fruits, broccoli, tomatoes, peppers, Brussels sprouts, green leafy vegetables, cauliflower, and potatoes, are the most food sources of this vitamin [5, 6]. Close to 80–90%

of AA is attracted to the gastrointestinal tract and circulates in leukocytes, plasma, red blood cells, and enters all tissues [7]. A high amount of L-ascorbic acid is discovered in the brain, leukocytes, hypophysis and adrenal glands, fluids, and eye tissues [8]. Plenty of analytical methods have been introduced for the detection and determination of AA. Spectrometry [9, 10], common titrimetric method [11], fluorimetry [12], chemiluminescence [13], enzymatic methods [14], capillary electrophoresis [15], and HPLC [16, 17] are the most common.

However, many of them, notwithstanding their reliability and accuracy, suffer from several limitations. For instance, high-performance liquid chromatographic (HPLC) methods are time-consuming and applying expensive grades of equipment, reagents, and eluents. Moreover, in comparison with other methods, because of their ease of operation, high sensitivity, short analysis times, non-toxic materials, relatively safe, reasonable costs, and the possibility of miniaturization as in vivo sensors, electroanalytical techniques are under regard [18, 19]. While several electrochemical techniques like amperometry and voltammetry are reported for detection and determination of the AA in various samples [12–15, 20–22], most of them suffer from low selectivity and

sensitivity, low linear concentration range, and high LOD. Li et al. [23] reported a study regarding the detection of AA using amperometric and a carbon paste electrode (CPE) modified with graphene-doped CPE (concentration range of 0.1–106 μM and a LOD = 0.07 μM). Recently, AA detection was carried out by Sha, Rinky, and Sushmee Badhulika using rGO/SnO₂/GCE [24]. The analytical performance of this electrode was assessed, with a concentration range of 400–1600 μM and a LOD of 38.7 μM . As previously mentioned, the TiO₂@CuO-rGO nanocomposites may be offering several potential applications in various fields like energy storage electromagnetic shielding, fuel cells, and electro-optical devices. The TiO₂@CuO-rGO nanocomposites can be a successful platform in designing an electrochemical sensor. Creating an effective platform to attain a stable electrochemical response is an important agent in the fabrication of a sensitive and selective electrochemical sensor. Among diverse types of electrodes, the glassy carbon electrode (GCE) has received remarkable interest due to its simplicity of fabrication, wide potential range, and low residual current and simple surface regeneration. In addition, using nanostructures has absorbed an enormous interest in modifying the activity of electrochemical sensors [24–31]. Reduced graphene oxide (rGO) has become a highly developing surface area in new research thanks to plenty of glorious characteristics like a large area, powerful mechanical strength, electrocatalytic properties, and great conductivity [25]. A mixture of the rGO with other nanomaterials such as magnetic NPs and metal oxide, with inherent unique properties, can result in simplifying electron transfer among redox systems and bulk electrode materials. Different kinds of nanostructures have been used for this purpose; recently, TiO₂ nanoparticles by having good dispersing properties, large surface area, and good biocompatibility have been widely applied for either electrochemical biosensor fabrication or mechanistic studies [18, 32, 33]. CuO is one of the most important intermediate metal oxides that have unique properties. These nanoparticles are one of the most important oxides in modern technology, and because they are easily available, they have received many regards and owing to their mechanical, optical, good electrocatalytic activity, and electrical properties, the use of these nanoparticles is increasing [18, 34, 35].

A combination of the TiO₂NPs, CuO, and rGO and manufacture of nanocomposites would be an appropriate selection to form an effective platform within the manufacture of a GCE as a selective and sensitive sensor. The main aim of this work is to present a new sensor based on TiO₂@CuO-rGO-modified glassy carbon electrode (TiO₂NP@CuO-rGO/GCE) for ultra-sensitive AA determination that has a good electrocatalytic activity to detect AA. The characterization and properties of TiO₂NP@CuO-rGO/GCE were investigated using several applied applications, and usual

techniques of the sensor were studied in human blood serum samples as the real sample.

Experimental section

Materials and instruments

Ascorbic acid, citric acid monohydrate, copper (II) nitrate hexahydrate (Cu(NO₃)₂·6H₂O), ethanol, and cetyl trimethyl ammonium bromide (CTAB) were purchased from Merck Company (<http://www.merck.com>) and Sinopharm Chemical Reagent Company (<http://en.reagent.com.cn/>) and were used without any further purification. By an ultrapure water system (Smart-2-Pure, TKACo, Germany), deionized water (DI) is ready.

Acetate buffer solutions and phosphate buffer (PB) were used as the supporting electrolyte. A solution consists of [Fe(CN)₆]³⁻⁴⁻ with a concentration of 0.5 mM, and KCl (1:1) with a concentration of 0.01 M was used as a redox probe. These solutions were prepared using NaH₂PO₄ and Na₂HPO₄ or CH₃COOH and CH₃COONa from Sinopharm Chemical Reagent Company. All other chemicals were of analytical grade and were used without any treatment. AA was dissolved in DI, and a solution containing 0.1 mM AA as a stock solution was obtained. The electrochemical evaluation was done using a PalmSens (Em state 3+, The Netherlands) Potentiostat. This instrument was in connection with common three-electrode setup including a Pt wire as an auxiliary electrode (Azar Electrode, Iran), an unmodified or modified GCE as a working electrode (Azar Electrode, Iran), and an Ag/AgCl (3 M KCl) as a reference (Azar Electrode, Iran). A Bel PHS3-BW pH/mV meter (made in Italy) was practical for pH measurements. The spectrum of Fourier transform infrared spectroscopy (FT-IR) was obtained through PerkinElmer/Lambda 25 and PerkinElmer/RXIFT-IR (USA), the morphology and structure of the layers were characterized by using X-ray diffraction (XRD) taken on a Philips X'Pert Pro (The Netherlands), and scanning electron microscope (SEM) images were obtained by using JSM-6700F (Japan). All testing was run under room temperature.

Synthesis of TiO₂NP@CuO-5 wt% rGO ternary nanocomposites

TiO₂ nanoparticles (NPs) were prepared by the solgel process [18]. In an ice bath, the TTIP (4.7 mL) was hydrolyzed by glacial acetic acid (9.0 mL). Then, under powerful stirring, DI (98.8 mL) was added dropwise to the mixture for 60 min. After sonicating for 60 min, a clear solution was obtained and stored for nucleation in a dark location of one night's duration. Afterward, for 12 h, the solution was heated at 70 °C. Ultimately, to form the TiO₂NP, the gel was dried

at 110 °C and annealed at 500 °C for 2 h. By the sol-gel process, a CuO shell was coated on the TiO₂ NPs. The synthesized TiO₂ NPs (0.5 g) were dispersed in a mixed solution of 30 mL of DI, 20 mL of ethanol, CTAB, and citric acid (2:1) aqueous solution for 15 min by ultrasonication. Then, under mechanical stirring, 1/86 g of Cu(NO₃)₂·6H₂O in 60 mL of DI was dropwise added to the dispersion TiO₂ NPs. To this solution, 10 mL of DI and 10 mL of ethanol mixed solution of 5 wt% of GO were added followed by sonication for 5 min to form a homogeneous suspension. Afterward, the reaction was carried out at room temperature for 2 h till it became a homogeneous solution. Next, it was dried at 130 °C for 24 h. Eventually, the core-shell TiO₂NP@CuO-5 wt% rGO ternary nanocomposites were sintered in a muffle furnace at 550 °C for 2 h [36].

Preparing the real samples

The human blood serum and samples as the real sample were prepared from the Blood Transfusion Organization (<http://www.tbtc.ir>) at Tehran, Iran. The samples were exposed to the ultrafiltration by lading them into a centrifugal filtration tube for 30 min at 5000 rpm. Afterward, the samples were attentively diluted with 0.1 M PBS (1:5) and given concentrations of the AA were added to 1 ml of the samples. Finally, 20.0 mL of each solution was pipetted separately and independently from the others in the electrochemical cell to the test. The DPV signals for each obtained solution were independently and separately evaluated by the modified GCE via the standard method.

Fabrication of TiO₂NP@CuO-rGO/GCE

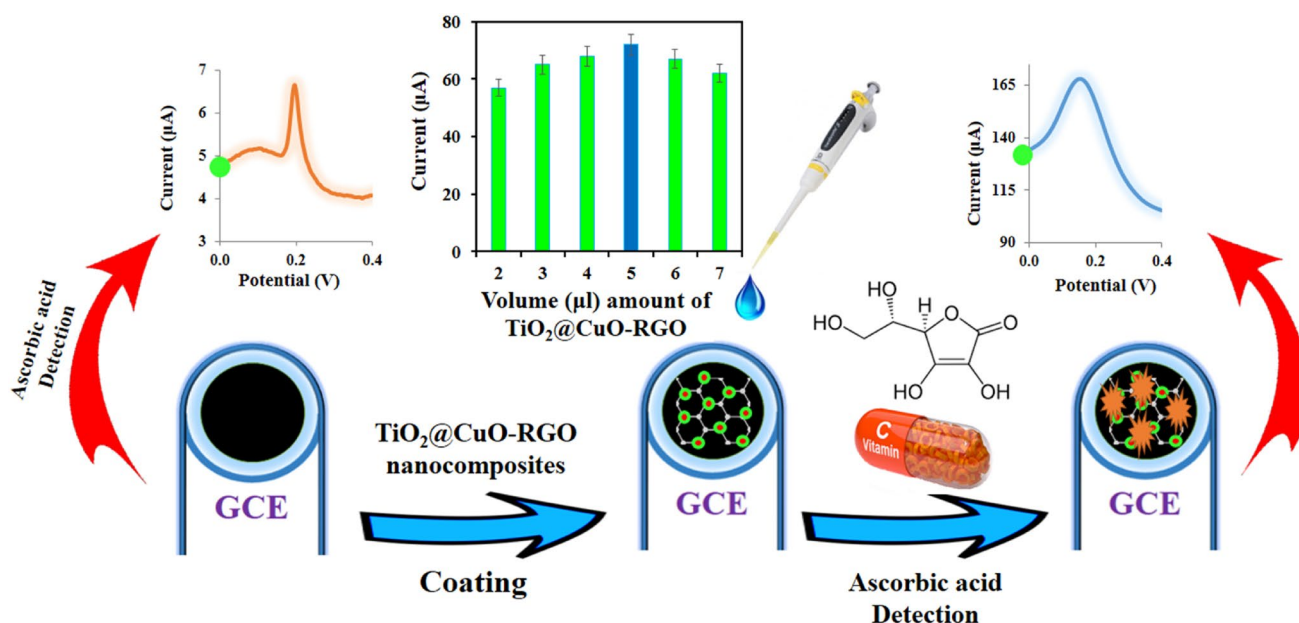
Before modification of the GCE, the bare GCE was polished to a mirror surface with alumina down to 0.05 μm, afterward cleaned ultrasonically in DI for 2 min, and eventually cleaned in an ultrasonic cleaner with DI and nitric acid (1:1). Then, GCE was washed with DI and dried under room temperature conditions to use.

5 μL TiO₂NP@CuO-rGO solution (suspension) of 1 mg mL⁻¹ concentration was drop-coated on a conductive GCE surface and then dried under ambient conditions. Finally, the modified electrode TiO₂NP@CuO-rGO/GCE was dried in air and stored at room temperature and used as the sensor for quantitative and qualitative measurements of the AA. The fabrication process of the sensor is displayed in Scheme 1.

Results

Choice of materials

Preparation of an effectual platform within the process of the electrode modification is perhaps a vital step. There are plenty of nanomaterials and various compounds to modify an electrode surface. One of the key factors in electrode modification is the use of economical reagent and non-toxic to create a simple and functional method to detect and measure the targets. In addition to high conductivity and large surface area, the combination of graphene with other nanomaterials such as MNPs and metal oxides generally



Scheme 1 A novel sensor by TiO₂NP@CuO-rGO/GCE

augments stability, catalytic activity, and sensing [18, 25, 37]. Here, with respect to the electronic characteristics of TiO₂ and GO [18] and semiconductor properties of CuO [18], a clever combination of the TiO₂NP, CuO, and GO to the synthesis of ternary nanocomposites pretends that they have the potential to raise electrochemical performance.

Reduced graphene oxide (rGO) has catalytic properties and relatively strong conducting in addition to the possibility and simplicity of use in miniaturized applications [25]. Also, the rGO in aqueous media can the plural on the surface of the electrode and conduct to a reduction in the efficient surface area [25]. In addition, several nanocomposites are reported by TiO₂NP, CuO, SnO₂, and graphene to combine the great supramolecular sensing potentials of them in the detection and determination of different targets [25]. This work shows the core-shell TiO₂NP@CuO-rGO ternary nanocomposites with particular capability in the detection and determination of different targets. Among plenty of nanomaterials, the clever combination of the TiO₂, CuO, and rGO as a modern nanocomposite by established unique properties can make a new and effective platform in the detection and determination of the AA.

So far, the different platform has been practiced in several electrochemical methods for the detection of AA. Several reported instances of them include a modified GCE with multi-walled carbon nanotubes (MWCNTs), 3D nitrogen-doped nanostructured carbons with hierarchical architectures, poly(xanthurenic acid)-MWCNTs composite, and a CPE modified with graphene-doped MWCNTs based on the simplest of the authors' knowledge; no report has been reported still on the TiO₂NP@CuO-rGO nanocomposite in the modification of the GCE for sensing of AA [21, 22].

Characterization of the TiO₂NP@CuO-rGO nanocomposite

The XRD analysis of TiO₂, CuO, TiO₂NP@CuO, and the synthesized TiO₂NP@CuO-rGO is shown in Fig. 1a. The peaks of the prepared CuO may be assigned to monoclinic symmetry of CuO [18] (JCPDS card No. 45-0937). Besides, a peak appears at about 28.53 attributed to (110) diffraction for Cu₂O phases [18] (JCPDS card No. 49-1830) in the nanosensors. The XRD patterns of titania nanoparticles show the usual diffraction patterns of pure anatase phase (JCPDS card no. 21-1217) [18]. All the broad XRD peaks also indicate that the nanosensors are composed of TiO₂ and CuO nanocrystallites. RGO incorporation was achieved in sharper signals which display higher crystalline structure [32]. And rGO signal about 2θ = 25.5° is not denoted which could be owing to the surface coverage by the TiO₂@CuO core-shell nanoparticles [18]. The results also display that rGO does not inhibit the formation of TiO₂@CuO core-shell crystallites. Similar

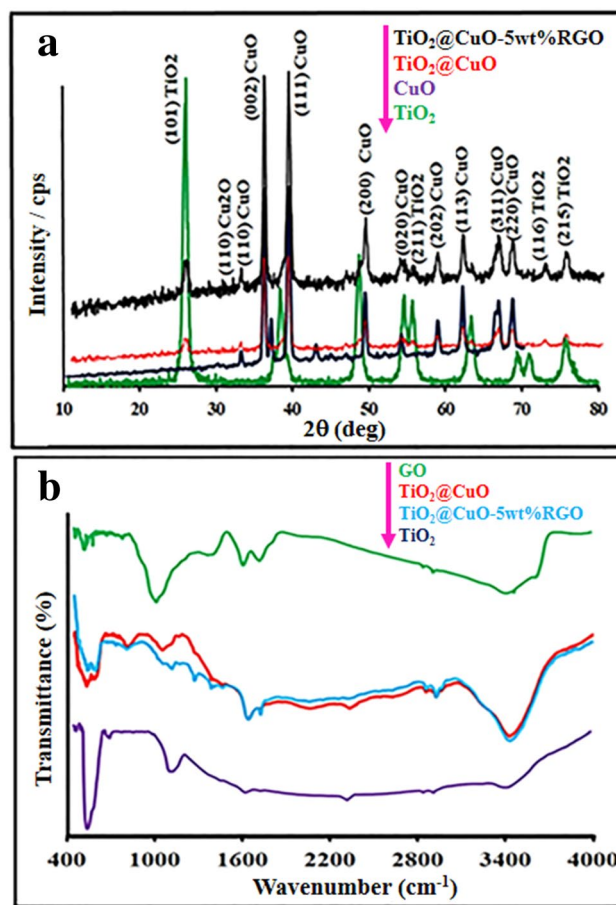


Fig. 1 a XRD patterns and b the FT-IR spectra

findings are shown for nanosensors, as shown in Fig. 1. Scherer's formula in Eq. (1) is used to compute the crystallite size:

$$D = \frac{k\lambda}{\beta \cos \theta} \quad (1)$$

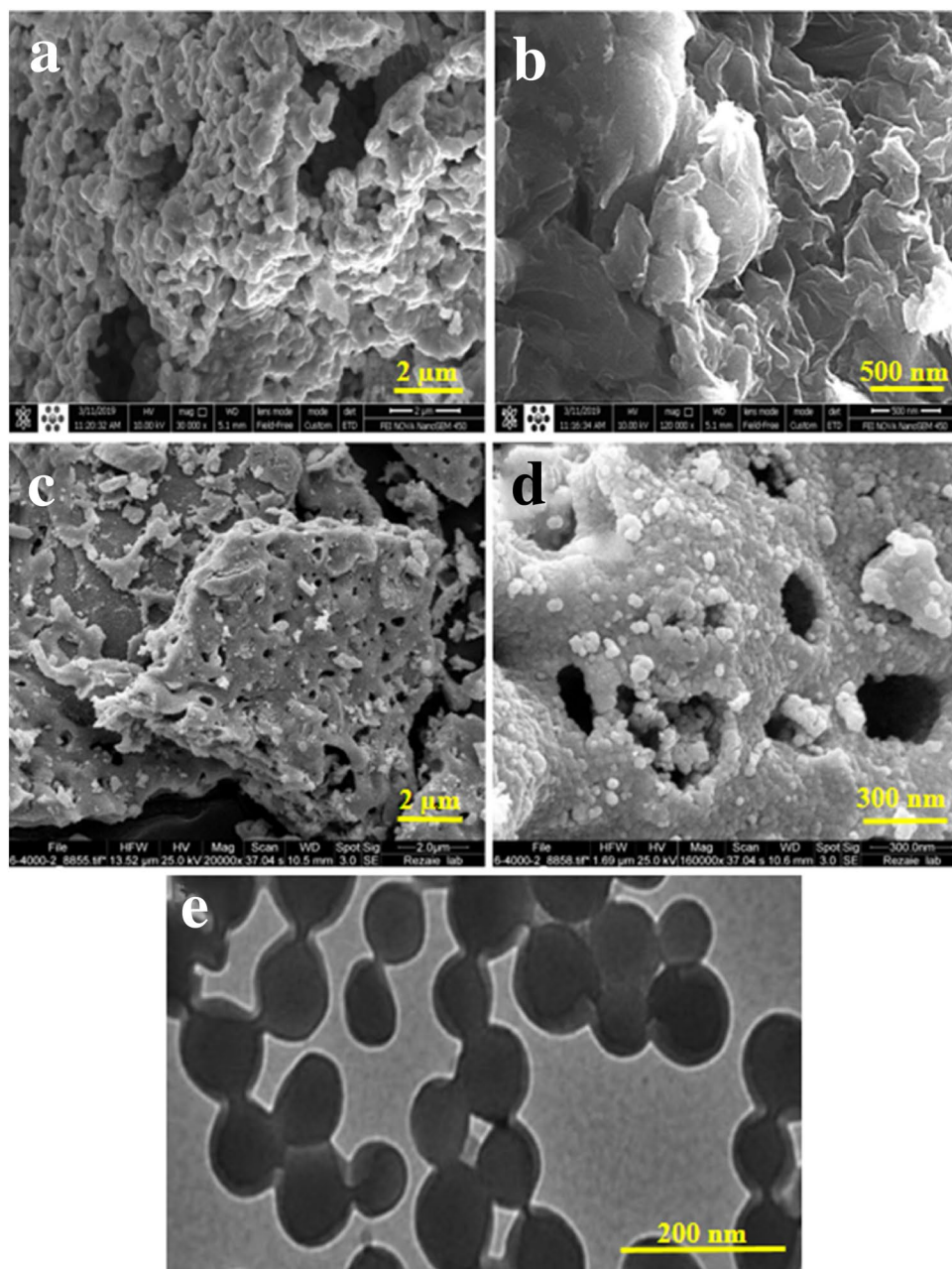
where λ is the wavelength of X-ray radiation, D is the crystallite size, $k=0.9$, used, and θ is the Bragg's angle [18]. The crystallite size, as displayed in Fig. 1, is in the range of 21–28, 23–29, 25–35, and 31–39 nm for TiO₂, CuO, TiO₂@CuO core-shell, and TiO₂NP@CuO-rGO nanostructures, respectively. In addition, interactions among functional groups in the synthesized product were examined briefly by the FT-IR spectrum, as displayed in Fig. 1B. The FT-IR spectra can reflect the functional groups of as-synthesized TiO₂, TiO₂@CuO, GO, and TiO₂NP@CuO-5wt% rGO nanostructures. The TiO₂NP@CuO-rGO nanocomposite displays a powerful absorption peak at about 573 and 535 cm⁻¹, which may be regarding the Cu–O and Ti–O vibration, respectively [18]. The band at 3422 cm⁻¹ corresponds to the O–H stretching vibration of the hydrogen-bonded

hydroxyl groups and the interlayer water molecules [33]. For the FT-IR spectrum of GO and $\text{TiO}_2\text{NP}@CuO$ -5 wt% rGO ternary nanocomposite, the stretching vibrations of C–O (1053 cm^{-1}), C–O–C (1101 cm^{-1}), C=O (1725 cm^{-1}), C–O (1384 cm^{-1}), and C=C (1634 cm^{-1}) confirm the formation of ternary nanocomposites during the solgel reaction. The bands at 2925 and 2858 cm^{-1} are the asymmetric CH_2 stretching and the symmetric CH_2 stretching. Stretching vibration peaks of C–O (alkoxy) and C–O (epoxy) are observed at 1270 cm^{-1} and 1454 cm^{-1} , respectively [18, 33].

Morphology of the composition

SEM was used for the investigation of the morphology of the synthesized $\text{TiO}_2\text{NP}@CuO$ -rGO nanostructure. Figure 2 displays the morphology of (a) CuO, (b) GO, (c) $\text{TiO}_2@CuO$, and (d) $\text{TiO}_2\text{NP}@CuO$ -rGO by SEM images. As it is shown, the GO nanosheets are uniformly decorated with $\text{TiO}_2@CuO$ core–shell. Indeed, the presence of graphene nanosheets supplies a very huge surface area for growth and formation of small $\text{TiO}_2@CuO$ core–shell nanoparticles with average particle sizes of about ~ 25 – 39 nm as well as suppression of agglomeration. By exfoliating naturally

Fig. 2 The recorded SEM images of the surface area for: **a** CuO, **b** GO, **c** $\text{TiO}_2\text{NP}@CuO$, **d** $\text{TiO}_2\text{NP}@CuO$ -rGO, and **e** TEM of $\text{TiO}_2\text{NP}@CuO$



occurring graphite, the GO was prepared as individual GO nanosheets or a few layers of GO. The chemical exfoliation of graphite to individual GO layers using powerful oxidizing factors has become the most usual and famous technique, which introduces oxygen functional groups [34, 38]. In addition, the presence of TiO_2 @CuO core-shell nanoparticles inhibits the stacking of the graphene nanosheets which is beneficial for the approachability of higher surface for high-performance nanosensors. Also, Fig. 2e shows that the TEM investigation reveals the shape of primary particles and the view of agglomeration. The nanoparticles are spherical in shape and show the core-shell-like structure. As we see in Fig. 2e, the spherical shape particles are there having some amount of agglomeration.

Electrochemical characterization of the $\text{TiO}_2\text{NP}@$ CuO-rGO/GCE

First, electrochemical behavior of the modified electrode was investigated by CV using $[\text{Fe}(\text{CN})_6]^{3-/4-}$ as a redox probe. Figure 3a shows the CVs recorded for (a) bare GCE, (b) $\text{TiO}_2\text{NP}@$ CuO/GCE, and (c) $\text{TiO}_2\text{NP}@$ CuO-rGO/GCE in 0.5 mM of $[\text{Fe}(\text{CN})_6]^{3-/4-}$ solution (1:1) containing 0.01 M KCl at a scan rate of 50 mV/s (potential window of -0.04 to 0.5 V). As displayed, two well-defined redox peaks with a peak-to-peak separation (ΔE_p) of about 86 mV is shown for the bare GCE. For the $\text{TiO}_2\text{NP}@$ CuO-rGO/GCE, ΔE_p is about 89 mV. As seen, after modification of GCE with $\text{TiO}_2\text{NP}@$ CuO-rGO/GCE, the peak current increased clearly (curve c) owing to the enhancement surface area and electrocatalytic activity of the electrode by $\text{TiO}_2\text{NP}@$

CuO-rGO/GCE of this nanocomposite toward oxidation of $[\text{Fe}(\text{CN})_6]^{3-/4-}$.

The electrochemical impedance spectroscopy (EIS) was used for further characterization of the modified GCE. In a frequency range of 0.1–10,000 Hz, these experiments were performed. The Nyquist diagrams obtained at 0.23 V are composed of a semicircular and a straight linear curve. The charge transfer resistance (R_{ct}) is a significant parameter in this technique to measure the kinetics of the redox probe at the GCE interface and display the substrate attachment to the modified GCE surface in each step of the modification process [18, 39, 40]. Figure 3B demonstrates the Nyquist plots obtained using bare GCE (a), $\text{TiO}_2\text{NP}@$ CuO/GCE (b), and $\text{TiO}_2\text{NP}@$ CuO-rGO/GCE (c) in a 0.5 mM $[\text{Fe}(\text{CN})_6]^{3-/4-}$ solution also containing 0.01 M of KCl. It can be observed that on the $\text{TiO}_2\text{NP}@$ CuO-rGO/GCE (curve c, $R_{ct} = 320 \Omega$) the value of R_{ct} is smaller than that of TiO_2 @CuO/GCE (curve b, $R_{ct} = 820 \Omega$) and bare GCE (curve a, $R_{ct} = 760 \Omega$).

This is owing to the great catalytic property of $\text{TiO}_2\text{NP}@$ CuO-rGO/GCE that formed a high electron conduction route among the electrode and $[\text{Fe}(\text{CN})_6]^{3-/4-}$. A reduction in the R_{ct} value attributed to the capability of high surface area ratio and excellent conductivity of the $\text{TiO}_2\text{NP}@$ CuO-rGO nanostructure.

In order to compare the surface area of the $\text{TiO}_2\text{NP}@$ CuO-rGO/GCE with bare GCE, the CVs plots of both electrode in the electrolyte solution (containing 0.5 mM $[\text{Fe}(\text{CN})_6]^{3-/4-}$ and 0.01 M of KCl) at various scan rates (ν) ranging from 0.01 V s^{-1} to 0.20 V s^{-1} were recorded. Based on Randles-Sevcik Eq. (2), the peak current is I_p (A), the

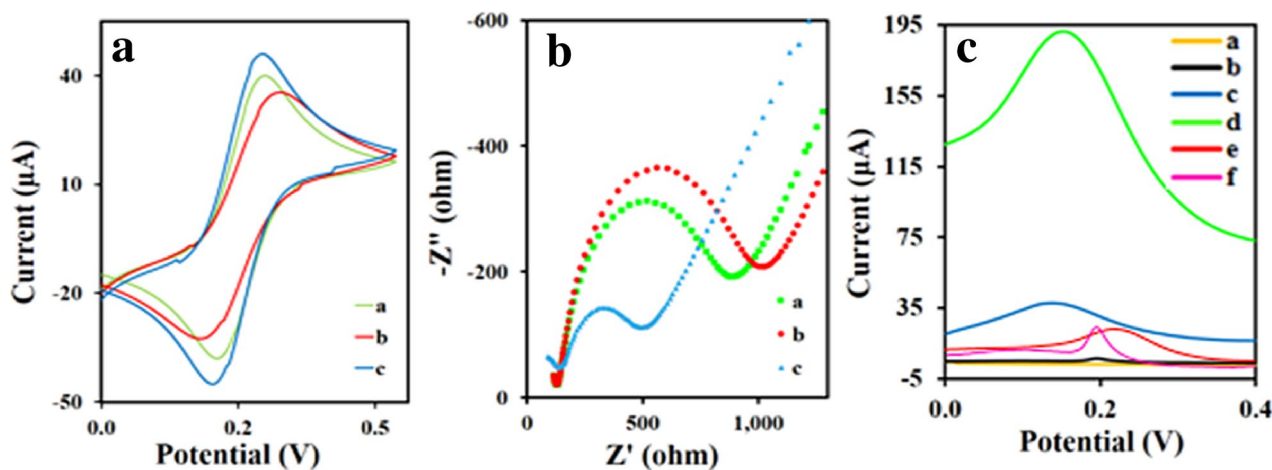


Fig. 3 **a** The CVs recorded in 0.5 mM $[\text{Fe}(\text{CN})_6]^{3-/4-}$ solution containing 0.01 M KCl (1:1) at a scan rate of 50 mV s^{-1} (a: bare GCE, b: $\text{TiO}_2\text{NP}@$ CuO/GCE, c: $\text{TiO}_2\text{NP}@$ CuO-rGO/GCE). **b** Electrochemical impedance spectra of (a: bare GCE, b: $\text{TiO}_2\text{NP}@$ CuO/GCE, c: $\text{TiO}_2\text{NP}@$ CuO-rGO/GCE) in 0.5 mM $[\text{Fe}(\text{CN})_6]^{3-/4-}$ solution containing 0.01 M KCl (1:1) supporting electrolyte. **c** Differential pulse

voltammograms of the glassy carbon electrode in PB solution with pH 7.0 as the bare glassy carbon electrode (a) and DPV recorded in PB solution with pH 7.0 as supporting electrolyte at bare GCE. Same solution containing $0.1 \mu\text{M}$ of AA (b) at bare GCE, (c) at $\text{TiO}_2\text{NP}@$ CuO/GCE, (d) at $\text{TiO}_2\text{NP}@$ CuO-rGO/GCE, (e) at CuO/GCE, and (f) $\text{TiO}_2\text{NP}/\text{GCE}$

number of transferred electrons is n , the diffusion coefficient is D ($\text{cm}^2 \text{s}^{-1}$), and the bulk concentration of the substrate is C_s (mol cm^{-3}). By considering the values of the equation slope, $n = 1$, $D = 7.6 \times 10^{-6} \text{ cm}^2 \text{ s}^{-1}$, and C_s of the redox probe [39, 40],

$$I_p = 2.69 \times 10^5 \times n^{3/2} \times A \times D^{1/2} \times C_s \times \nu^{1/2}. \quad (2)$$

The calculated A value of the modified electrode ($\text{TiO}_2\text{NP@CuO-rGO/GCE}$) was calculated to be 1.30 cm^2 which is higher than the surface area of the bare GCE (0.6 cm^2).

Effect of modification of the GCE with $\text{TiO}_2\text{NP@CuO-rGO}$ on the analytical signal

The differential pulse voltammogram (DPV) recorded in PBS (pH 7.0) as the supporting electrolyte using non-modified GCE (a), DPVs recorded in the same buffer solution containing $0.1 \mu\text{M}$ AA using bare GCE (b), $\text{TiO}_2\text@CuO/GCE$ (c), $\text{TiO}_2\text{NP@CuO-rGO/GCE}$ (d), CuO/GCE (e), and $\text{TiO}_2\text{NP/GCE}$ (f) at 100 mV s^{-1} are illustrated in Fig. 3c. Obviously, no redox peaks could be observed in the blank samples. As can be seen, for both modified electrodes peak current is higher than that of non-modified GCE. The $\text{TiO}_2\text{NP@CuO-rGO/GCE}$ -modified electrode showed a larger and well-defined peak current by less positive E_p .

Effect of scan rate

The influence of the potential scan rate on the CV of AA using $\text{TiO}_2\text{NP@CuO-rGO/GCE}$ in PBS (pH 7.0) containing $1.0 \mu\text{M}$ AA at different scan rates in the range of $40\text{--}200 \text{ mVs}^{-1}$ is indicated in Fig. 4A. A linear relationship between anodic peak current (I_p) and scan rate over the potential sweep rate range of $40\text{--}200 \text{ mV s}^{-1}$ ($I_p = 0.0215 \nu + 20.60$ with $R^2 = 0.9967$) displays the adsorptive nature processes of the electrochemical oxidation of AA (Fig. 4Aa). This linear behavior was likewise seen for $\log I_p$ versus $\log \nu$ with a slope of 0.6185 ($\log I_p = 0.6185 \log \nu + 0.4091$ with $R^2 = 0.997$) (Fig. 4Ab), indicating the diffusion-controlled oxidation of AA onto the modified GCE. In addition, the linear relation between E_p and $\log \nu$ of $E_p = 0.0957 \log \nu + 0.0611$ with $R^2 = 0.9917$ (Fig. 4Ac) indicates that by increasing potential sweep rate, E_p shifts to more positive values, showing a limitation in the kinetic of electrochemical AA oxidation which is indicating an irreversible process.

Effect of pH

Influence of pH on the voltammetric treatment of AA, in the solutions containing 0.1 M buffer and $10.0 \mu\text{M}$ AA at a pH range of 6.5 to 8.0 , was investigated using cyclic

voltammetric method. The dependences of peak potential (E_p) and peak current (I_p) on pH are observed in Fig. 4B. As seen, with the increase in the pH, the peak current increased with the highest current happening at pH 7.0 and decreases after pH 7.0 (Fig. 4Ba). It was revealed that the anodic peak current (I_p) in pH 7.0 is higher than that in other pHs.

In addition, for the plot of E_p versus pH (Fig. 4Bb), it is indicated that by increasing pH from 6.5 to 8.0 , the E_p decreases and there is a linear relation between pH and E_p by the slope of 0.061 V/pH . This slope displays $2e^- - 2H^+$ electrochemical oxidation of AA in this pH range (Scheme 2S). Due to more reproducible findings and higher current at pH 7.0, it has been chosen as the optimum value for AA detection and determination.

Performance characteristics

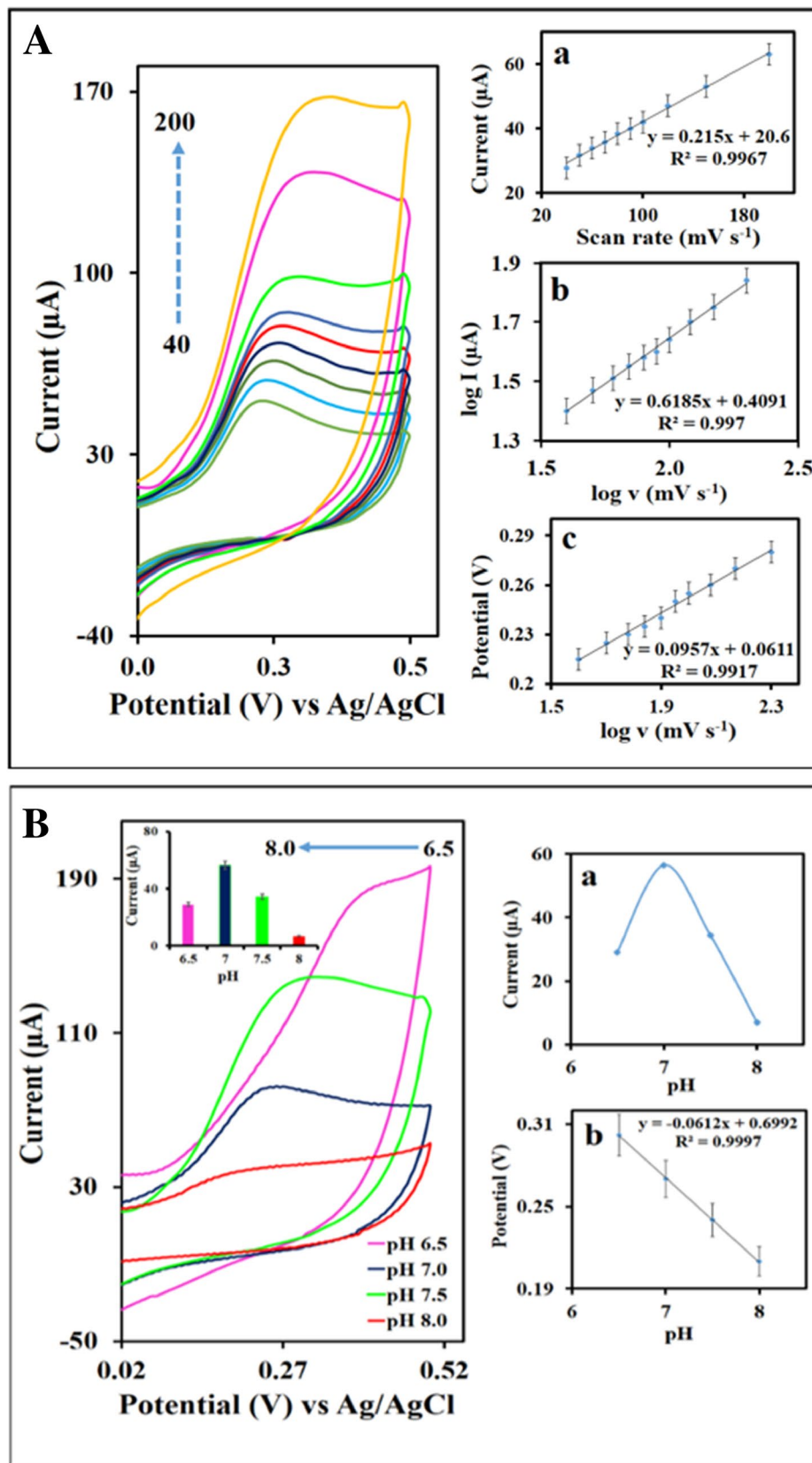
Stability and repeatability of the electrode

The modified GCE was stable, until after 12 days if it preserved in a closed container. The stability of the proposed modified GCE was investigated by recording DPV of $1.0 \mu\text{M}$ AA, every 3 days. The results showed that the electrode protected $87.0\% \pm 1.5$ of its original peak current (Fig. 5a), resulting in a standard deviation of 3.0% . This displays the long-term stability of the sensor. The repeatability of the modified GCE was calculated by the determination of the oxidation peak currents for five replicate DPVs on a PBS at pH 7.0 containing $1.0 \mu\text{M}$ AA. The relative standard deviation was found to be 3.4% , which is a great result, demonstrating the compatibility of the $\text{TiO}_2\text{NP@CuO-rGO/GCE}$ for applications in real analysis (Fig. 5b).

Voltammetric determination of ascorbic acid

Figure 6 displays the DPV curves of AA at different concentrations in 0.1 M PBS with pH 7.0 and corresponding analytical calibration plot. Based on these results, a good linearity relationship was obtained between the oxidation current signals and the log of the AA concentration (Fig. 6a). The regression equation of I_p (μA) = $11.542 \log C$ (nM) + 26.197 ($R^2 = 0.9926$) for 10.0 pM to $10.0 \mu\text{M}$ of AA was achieved. The LOD of the strategy was concluded to be 3.0 pM based on the $S/N = 3$. In addition, electrochemical sensitivity is used to make this electrode easier to compare with other electrodes, which actually shows the actual active surface area of the GCE as shown in Fig. 6b; the results reflect that the method has good sensitivity. A comparison of the results by the proposed electrode with those obtained previously indicates that it produces comparable or even better findings in terms of determination, LOD, and linear ranges for AA concentration (Table 1).

Fig. 4 **a** CVs of $\text{TiO}_2\text{NP}@$ $\text{CuO-rGO}/\text{GCE}$ buffer solution (pH 7.0) containing $1.0 \mu\text{M}$ AA at various scan rates including: 40, 50, 60, 70, 80, 90, 100, 120, 150, and 200 mV s^{-1} . **a** Variation of the I versus v , **b** variation of the $\log I$ versus $\log v$, and **c** E versus $\log v$. **B** Cyclic voltammograms of $\text{TiO}_2\text{NP}@$ $\text{CuO-rGO}/\text{GCE}$ containing $10.0 \mu\text{M}$ AA recorded from pH 6.5–8.0 at a scan rate of 100 mV s^{-1} . **a** Variation of the I_{pa} versus pH and **b** the E_{pa} versus pH



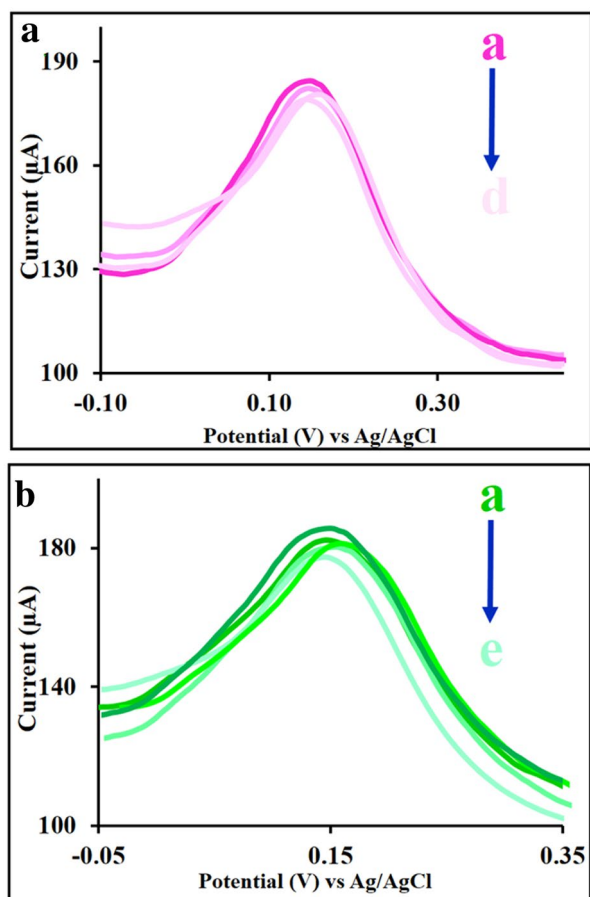


Fig. 5 The recorded DPVs of the $\text{TiO}_2\text{NP@CuO-rGO/GCE}$ in containing $1.0 \mu\text{mol L}^{-1}$ AA solution in PBS 0.1 mol L^{-1} ($\text{pH}=7.0$) at **a** 12-day period and signal were recorded every 3 days and **b** recording five replicate DPVs

The electrode also offers many advantages, including a low LOD and a wide linear dynamic range, without using toxic reagents, ease of use, high stability, satisfactory selectivity, good sensitivity, repeatability, reproducibility, high speed of analysis, and low cost.

These satisfactory results can be regarded as some important agents; (1) utilizing the rGO as a particular structure with excellent properties such as unique electronic and conducting properties, large active surface area; (2) using the $\text{TiO}_2\text{@CuO}$ core-shell nanostructure with unique inherent properties in the nanocomposite; (3) the capability of the synthesized nanocomposite as an effective platform in increased surface area, high conductivity, and catalytic activity enhancement; and (4) preparation of the active sites on the sensor surface which causes a proper puissance of the AA oxidation on the surface.

Generally, a special and clever combination of those three unique materials makes a high-porous nanocomposite on the GCE surface to organize active sites for the significant oxidation reaction of the AA.

Interference studies

The influences of different interfering species on AA detection in the presence of several organic compounds and inorganic ions as probabilistic interferences were estimated. The tolerance limit was defined as the concentration ratio of interference AA causing less than $\pm 5.0\%$ relative error. The results are demonstrated as follows: The tolerance limit of additives to $1.0 \mu\text{M}$ of AA was $300 \mu\text{M}$ of Na^+ , K^+ , and Cl^- ; $200 \mu\text{M}$ of Mg^{2+} and Ca^{2+} , $100 \mu\text{M}$ of glucose and fructose, $60 \mu\text{M}$ of valine, $60 \mu\text{M}$ of glycine, L-cysteine, and L-glutamic acid, $100 \mu\text{M}$ of citric acid, $200 \mu\text{M}$ of SO_4^{2-} , $150 \mu\text{M}$ of NO_3^- , and $20 \mu\text{M}$ for uric acid (Fig. 7). In addition, the histogram of the peak current responses in the presence of interferences without AA and with AA is shown in Fig. 7c. Therefore, it was found that these substrates did not interfere with $1.0 \mu\text{M}$ of AA detection regarding the strategy. The histogram of the change of concentration versus various probabilistic interferences toward AA is displayed in Fig. 7b. And the histogram of the peak current responses in the presence of interferences without AA and with AA is shown in Fig. 7c.

These satisfactory results show that the ternary nanocomposite-modified glassy carbon electrode has unrivaled properties that can be an excellent selection in the AA detection in some samples with a complex matrix.

AA determination in real samples

To evaluate the applicability of this electrode in real analysis, after diluting the samples with the supporting electrolyte, ascorbic acid (AA) was analyzed in blood serum samples. The standard addition method was used to estimate the concentration of AA in the samples. The percentages of the recovery values were calculated by comparing the concentrations got from the samples with actually added concentrations. Also, the RSD and recovery of AA assay in blood serum (Table 2) were assessed from three replicates at three nominal concentrations. The recoveries ranged from 92.5 to 105.0%, which became visible that the proposed method had good accuracy and a satisfactory potential in the practical sample analysis.

Conclusions

A novel modified electrode was introduced for the detection of AA by an electrochemical method. The $\text{TiO}_2\text{NP@CuO-rGO/GCE}$ was found to be excellent for AA determination. By having a wide linear range, low LOD, good electrocatalytic activity, high stability, and reproducibility in physiological pH, the proposed sensor has an excellent performance potential for the applied determination of AA.

Fig. 6 Differential pulse voltammograms of TiO₂NP@CuO-rGO/GCE in different AA concentrations in the range of 10.0 pM to 10.0 μM (a–h), **a** the plot of I_{pa} versus AA concentrations in the range of 0, 10.0 pM, 0.1 nM, 1.0 nM, 10.0 nM, 100.0 nM, 1.0 μM, and 10.0 μM. **b** Current density versus the same AA concentrations in an electrolyte: 0.1 M PBS at pH=7.0 (the DPV parameters: E step=5.0 mV, E pulse=60.0 mV, t pulse=0.02 s with scan rate = 100.0 mV s⁻¹)

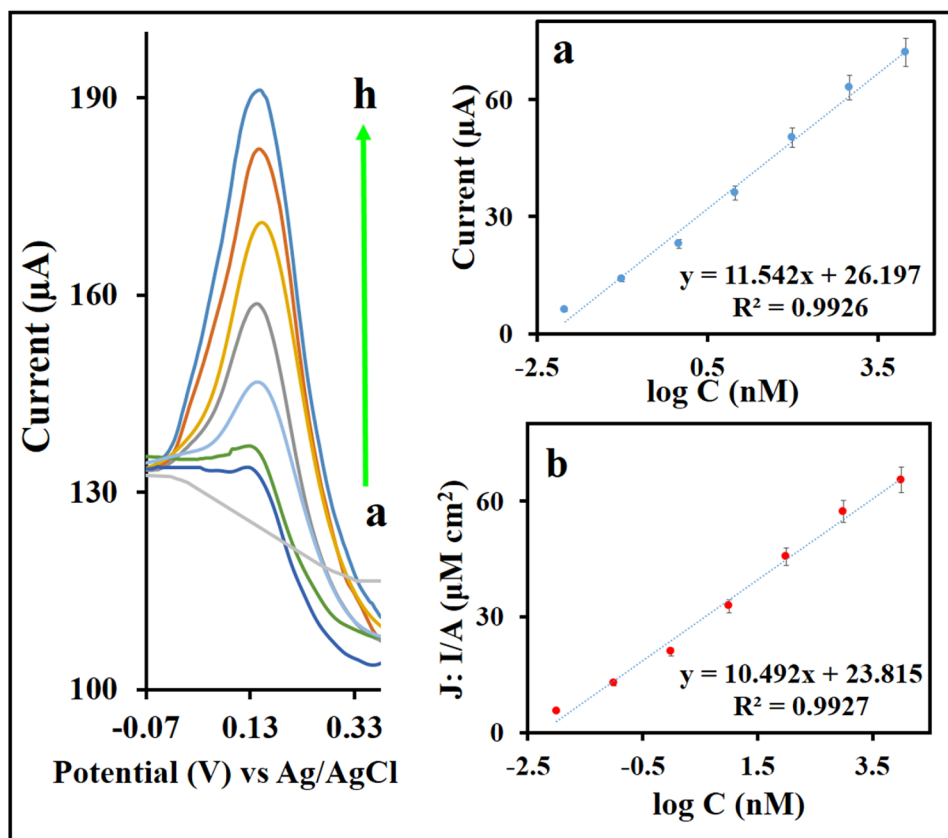


Table 1 Comparison of analytical parameters for determination of AA at various modified electrodes

Electrode	Technique	Linear range (μM)	LOD (μM)	pH	Potential (V)	References
CPE ^a /MWCNTs ^b	Voltammetric (SWV)	0.02–140.0	0.091	6.0	0.4	[41]
Graphene-doped/CPE	Amperometric	0.1–106	0.07	7.0	–	[23]
Poly(xanthurenic acid)–MWCNTs/GCE ^c	Amperometric and voltammetry (SWV)	1.0–1520	0.1	7.0	0.3	[21]
3D-NNCsHAs ^d /GCE	Amperometric	10–4410	1	7.0	–	[42]
Carbon nanotube fiber microelectrode	Voltammetry (DPV)	50–1000	10	7.4	–0.06	[43]
PAN-ABSA ^e /GCE	Voltammetry (DPV)	35–175	7.5	6.8	0.18	[44]
TiO ₂ /rGO	Amperometric	25–725	1.19	7.0	–	[38]
Gr ink	Voltammetry (SWV)	50–1000	17.8	7.4	0.0	[45]
rGO/SnO ₂ /GCE	Voltammetry (DPV)	400–1600	38.7	7.0	0.22–0.32	[24]
BN ^f /GCE	Voltammetry (DPV)	30–1000	3.77	6.0	0.11	[46]
Graphene/Pt/GCE	Amperometric	0.15–34.4	0.15	7.0	–	[47]
CL-TiN ^g /GCE	Voltammetry (DPV)	50–1500	1.52	7.0	0.21	[48]
TiO ₂ NP@CuO-rGO/GCE	Voltammetry (DPV)	0.00001–10	0.000003	7.0	0.15	This work

^aCarbon paste electrode

^bMultiwall carbon nanotubes

^cGlassy carbon electrode

^dThree-dimensional nitrogen-doped nanostructured carbons with hierarchical architectures

^ePolyaniline nanonetworks on *p*-aminobenzene sulfonic acid functionalized

^fFlake hexagonal boron nitride

^gChrysanthemum-like titanium nitride

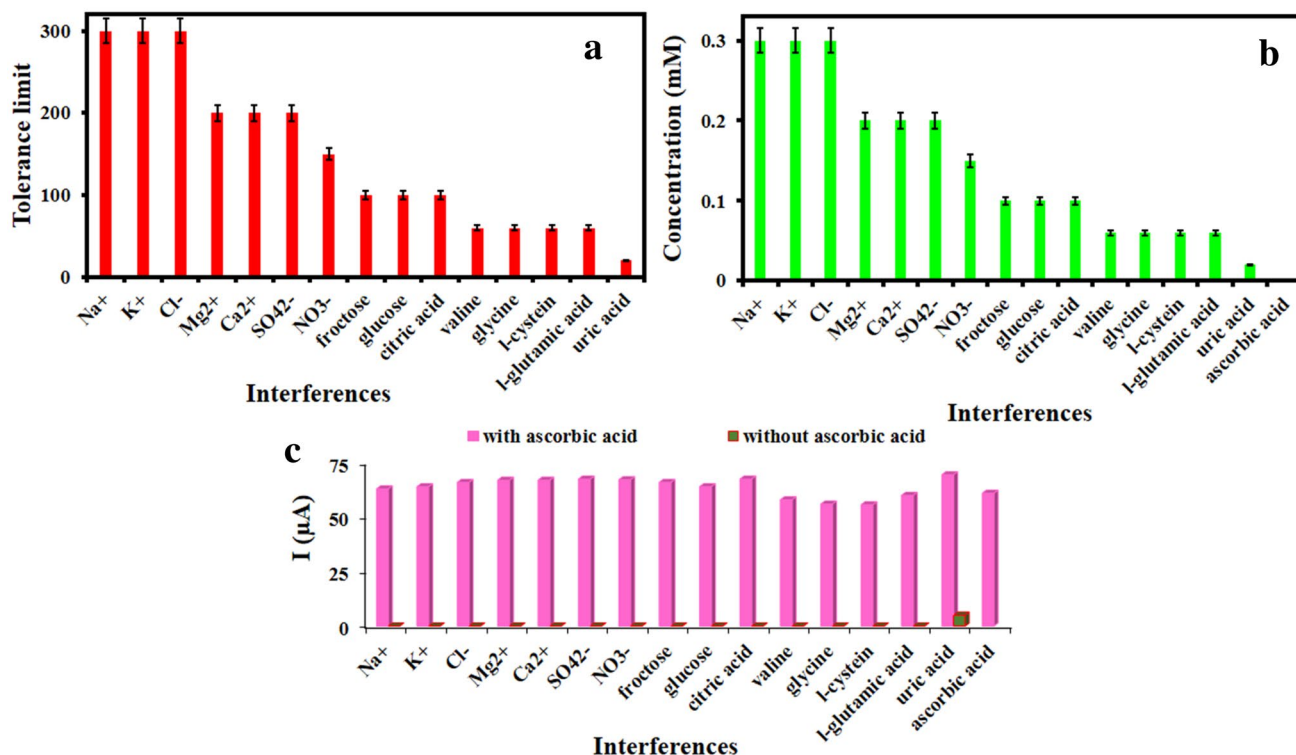


Fig. 7 Histogram of the change of **a** tolerance limit versus the interference and **b** concentration versus different probable interferences (1.0 μM AA, 0.3 mM for Na^+ , 0.3 mM for K^+ , 0.3 mM for Cl^- , 0.2 mM for Mg^{2+} , 0.2 mM for Ca^{2+} , 0.1 mM for glucose, 0.1 mM for fructose, 0.06 mM for valine, 0.06 mM for glycine, 0.06 mM

for L-cysteine, 0.06 mM for L-glutamic acid, 0.1 mM for citric acid, 0.2 mM for SO_4^{2-} , 0.15 mM for NO_3^- , and 20 μM for uric acid) and (C) peak current responses in the presence of interferences without AA and with AA

Table 2 Determination of AA in blood serum samples

No.	Primary (μM)	AA added (nM)	AA found (nM)	Recovery (%)
1	–	0.0	0.09	100.4 (1.5)
2	–	4.0	3.7	92.5 (3.5)
3	–	8.0	7.9	98.7 (4.1)
4	–	12.0	12.6	105.0 (2.8)
5	–	50.0	48.6	97.2 (3.2)
6	–	500.0	508.5	101.7 (2.5)

It had been successfully practiced for the determination of AA in human blood serum samples. The excellent potential application of the sensor may extend as a promising tool for use in pharmacokinetic analyses, quality control, and routine clinical tests.

References

- M. Ha, F. Graham, C. D'Souza, W. Muller, S. Igdoura, H. Schellhorn, *Genomics* **83**, 482 (2004)
- B. Peterkofsky, *Am. J. Clin. Nutr.* **54**, 1135S (1991)
- B. Eipper, D. Stoffers, R. Mains, *Annu. Rev. Neurosci.* **15**, 57 (1992)
- C. Rebouche, *Am. J. Clin. Nutr.* **54**, 1147S (1991)
- K. Phillips, M. Tarragó-Trani, S. Gebhardt, J. Exler, K. Patterson, D. Haytowitz, P. Pehrsson, J. Holden, *J Food Compos Anal.* **23**, 253 (2010)
- A. Pisoschi, A. Pop, G. Negulescu, A. Pisoschi, *Molecules* **16**, 5751 (2011)
- J. Olson, R. Hodges, *Am. J. Clin. Nutr.* **45**, 693 (1987)
- D. Hornig, *Ann. N. Y. Acad. Sci.* **258**, 103 (1975)
- J. Fan, C. Ye, S. Feng, G. Zhang, J. Wang, *Talanta* **50**, 893 (1999)
- W. Zeng, F. Martinuzzi, A. MacGregor, *J. Pharm. Biomed. Anal.* **36**, 1107 (2005)
- S. Kirk, S. Ronald, *Pearson's Composition and Analysis of Foods*, 9th edn. (Longman Group Ltd., London, 1991)
- A. Lopez-Anaya, M. Mayersohn, *Clin. Chem.* **33**, 1874 (1987)
- T. Pérez-Ruíz, C. Martínez-Lozano, A. Sanz, *Anal. Chim. Acta* **308**, 299 (1995)
- W. Lee, S. Roberts, R. Labbe, *Clin. Chem.* **43**, 154 (1997)
- T. Wu, Y. Guan, J. Ye, *Food Chem.* **100**, 1573 (2007)
- N. Furusawa, *Food Control* **12**, 27 (2001)
- R. Kandár, P. Drábková, R. Hampl, *J. Chromatogr. B* **879**, 2834 (2011)
- M. Ghanbari, F. Shahdost-Fard, M. Rostami, A. Khoshroo, A. Sobhani-Nasab, N. Gholipour, H. Salehzadeh, M. Ganjali, M. Rahimi-Nasrabadi, F. Ahmadi, *Microchim. Acta* **186**, 698 (2019)

19. M. Ghanbari, P. Sharafi, S. Nayeboossadr, Z. Norouzi, *Microchim. Acta* **187**, 1 (2020)
20. S. Ly, J. Chae, Y. Jung, W. Jung, H. Lee, S. Lee, *Nahrung/Food* **48**, 201 (2004)
21. K.-C. Lin, P.-C. Yeh, S.-M. Chen, *Int. J. Electrochem. Sci.* **7**, 12752 (2012)
22. A. Pisoschi, A. Pop, A. Serban, C. Fafaneata, *Electrochim. Acta* **121**, 443 (2014)
23. F. Li, J. Li, Y. Feng, L. Yang, Z. Du, *Sens. Actuators B Chem.* **157**, 110 (2011)
24. R. Sha, S. Badhulika, *J. Electroanal. Chem.* **816**, 30 (2018)
25. M. Ghanbari, F. Shahdost-Fard, H. Salehzadeh, M. Ganjali, M. Iman, M. Rahimi-Nasrabadi, F. Ahmadi, *Microchim. Acta* **186**, 641 (2019)
26. H. Jin, C. Zhao, R. Gui, X. Gao, Z. Wang, *Anal. Chim. Acta* **1025**, 154 (2018)
27. X. Gao, R. Gui, K. Xu, H. Guo, H. Jin, Z. Wang, *New J. Chem.* **42**, 14796 (2018)
28. H. Jin, H. Guo, X. Gao, R. Gui, *Sens. Actuators B Chem.* **277**, 14 (2018)
29. Y. Sun, X. Jiang, H. Jin, R. Gui, *Anal. Chim. Acta* **1083**, 101 (2019)
30. M. Ghanbari, M. Rahimi-Nasrabadi, H. Sobati, *Anal. Bioanal. Electrochem.* **11**, 189 (2019)
31. M. Ghanbari, Z. Norouzi, *Microchem. J.* **157**, 105098 (2020)
32. J. Shi, W. Leng, W. Zhu, J. Zhang, C. Cao, *Chem. Eng. Technol.* **29**, 146 (2006)
33. F. Harraz, M. Faisal, A. Ismail, S. Al-Sayari, A. Al-Salami, A. Al-Hajry, M. Al-Assiri, *J. Electroanal. Chem.* **832**, 225 (2019)
34. X. Li, W. Cai, L. Colombo, R. Ruoff, *Nano Lett.* **9**, 4268 (2009)
35. X. Gao, R. Gui, H. Guo, Z. Wang, Q. Liu, *Sens. Actuators B Chem.* **285**, 201 (2019)
36. N. Ibrayev, A. Zhumabekov, S. Ghyngazov, E. Lysenko, *Mater. Res. Express* **6**, 125036 (2019)
37. M. Ghanbari, A. Khoshroo, H. Sobati, M. Ganjali, M. Rahimi-Nasrabadi, F. Ahmadi, *Microchem. J.* **147**, 198 (2019)
38. W. Hummers, R. Offeman, *J. Am. Chem. Soc.* **80**, 1339 (1958)
39. M. Ghanbari, F. Shahdost-fard, A. Khoshroo, M. Rahimi-Nasrabadi, M. Ganjali, M. Wysokowski, T. Rebiś, S. Żółtowska-Aksamitowska, T. Jesionowski, P. Rahimi, Y. Joseph, H. Ehrlich, *Microchim. Acta* **186**, 438 (2019)
40. M. Ghanbari, Z. Norouzi, M. Ghanbari, *Microchem. J.* **156**, 104994 (2020)
41. M. Keyvanfard, R. Shakeri, H. Karimi-Maleh, K. Alizad, *Mater. Sci. Eng. C* **33**, 811 (2013)
42. Y. Hei, X. Li, X. Zhou, J. Liu, M. Hassan, S. Zhang, Y. Yang, X. Bo, H. Wang, M. Zhou, *Anal. Chim. Acta* **1029**, 15 (2018)
43. L. Zhang, F. Liu, X. Sun, G. Wei, Y. Tian, Z. Liu, R. Huang, Y. Yu, H. Peng, *Anal. Chem.* **89**, 1831 (2017)
44. L. Zhang, C. Zhang, J. Lian, *Biosens. Bioelectron.* **24**, 690 (2008)
45. L. Fu, A. Wang, G. Lai, W. Su, F. Malherbe, J. Yu, C. Lin, A. Yu, *Talanta* **180**, 248 (2018)
46. Q. Li, C. Huo, K. Yi, L. Zhou, L. Su, X. Hou, *Sens. Actuators B Chem.* **260**, 346 (2018)
47. C. Sun, H. Lee, J. Yang, C. Wu, *Biosens. Bioelectron.* **26**, 3450 (2011)
48. L. Zhang, J. Feng, K. Chou, L. Su, X. Hou, *J. Electroanal. Chem.* **803**, 11 (2017)